



Subscriber access provided by the Research Library | Los Alamos National Laboratory

# Communication

# Isotope Effect in Bilayer WSe

Wei Wu, Mayra Daniela Morales-Acosta, Yongqiang Wang, and Michael Thompson Pettes

Nano Lett., Just Accepted Manuscript • DOI: 10.1021/acs.nanolett.8b04269 • Publication Date (Web): 12 Feb 2019

Downloaded from http://pubs.acs.org on February 15, 2019

#### **Just Accepted**

"Just Accepted" manuscripts have been peer-reviewed and accepted for publication. They are posted online prior to technical editing, formatting for publication and author proofing. The American Chemical Society provides "Just Accepted" as a service to the research community to expedite the dissemination of scientific material as soon as possible after acceptance. "Just Accepted" manuscripts appear in full in PDF format accompanied by an HTML abstract. "Just Accepted" manuscripts have been fully peer reviewed, but should not be considered the official version of record. They are citable by the Digital Object Identifier (DOI®). "Just Accepted" is an optional service offered to authors. Therefore, the "Just Accepted" Web site may not include all articles that will be published in the journal. After a manuscript is technically edited and formatted, it will be removed from the "Just Accepted" Web site and published as an ASAP article. Note that technical editing may introduce minor changes to the manuscript text and/or graphics which could affect content, and all legal disclaimers and ethical guidelines that apply to the journal pertain. ACS cannot be held responsible for errors or consequences arising from the use of information contained in these "Just Accepted" manuscripts.



# Isotope Effect in Bilayer WSe<sub>2</sub>

#### **Authors**

Wei Wu<sup>1,2</sup>, Mayra Daniela Morales-Acosta<sup>2</sup>, Yongqiang Wang,<sup>3,4</sup> Michael Thompson Pettes<sup>1,2,4,\*</sup>

#### **Affiliations**

<sup>1</sup>Department of Mechanical Engineering, University of Connecticut, Storrs, Connecticut 06269, United States

<sup>2</sup>Institute of Materials Science, University of Connecticut, Storrs, Connecticut 06269, United States

<sup>3</sup>Materials Science and Technology Division, Los Alamos National Laboratory, Los Alamos, New Mexico 87545, United States

<sup>4</sup>Center for Integrated Nanotechnologies (CINT), Materials Physics and Applications Division, Los Alamos National Laboratory, Los Alamos, New Mexico 87545, United States

\*Corresponding Author, E-mail: pettesmt@lanl.gov

### **Keywords**

Isotope engineering, band gap engineering, tungsten diselenide, transition metal dichalcogenide, photoluminescence, Raman.

#### **Abstract**

Isotopes of an element have the same electron number but differ in neutron number and atomic mass. However, due to the thickness-dependent properties in MX<sub>2</sub> (M=Mo, W; X=S, Se, Te) transition metal dichalcogenides (TMDs), the isotopic effect in atomically-thin TMDs still

remains unclear especially for phonon-assisted indirect excitonic transitions. Here, we report the first observation of the isotope effect on the electronic and vibrational properties of a TMD material, using naturally abundant  $^{NA}W^{NA}Se_2$  and isotopically pure bilayer  $^{186}W^{80}Se_2$  single crystals over a temperature range of 4.4–300 K. We demonstrate a higher and nearly temperature independent optical band gap energy in bilayer  $^{186}W^{80}Se_2$  than in  $^{NA}W^{NA}Se_2$  (3.9 ± 0.7 meV from 4.41 K to 300 K), which is surprising as isotopes are neutral impurities. Phonon energies decrease in the isotopically pure crystal due to the atomic mass dependence of harmonic oscillations, with correspondingly longer  $E_{2g}$  and  $A^2_{1g}$  phonon lifetimes than in the naturally abundant sample. The change in electronic band gap renormalization energy is postulated as being the dominant mechanism responsible for the change in optical emission spectra.

## **Main Text**

With the discovery of graphene<sup>1</sup>, the atomically thin materials receive interest continuously. A wide application in electronics<sup>2-5</sup>, optoelectronics<sup>6-11</sup> and quantum phononics<sup>12-16</sup> has been achieved with the expansion of this class materials to the MX<sub>2</sub> (M=Mo, W; X=S, Se, Te) transition metal dichalcogenides (TMDs) possessing large band gaps compared with zero-gap graphene. TMDs are a group of materials consisting of three atom-thick layers with transition metals covalently bonded with chalcogens in trigonal prismatic coordination geometry, and adjacent layers bonded by relatively weak van der Waals interactions. Compared to bulk materials, atomically-thin TMDs offer size and tunability advantages over traditional materials as the requirement for miniaturization of electronic and optical devices<sup>6, 7, 17</sup>, especially as their optoelectronic and vibrational properties are highly dependent on layer thickness<sup>18, 19</sup>. Thus, the precise manipulation of electron and phonon band structure in atomically-thin TMDs materials is

the key to widespread adoption in applications including energy conversion<sup>20</sup>. Reversible modification of the electronic band gap in mono- and bi-layer crystals of MoS<sub>2</sub><sup>21</sup> and WSe<sub>2</sub><sup>10, 22</sup> has been demonstrated via strain<sup>23</sup>, in which bilayer WSe<sub>2</sub> showed a two-orders of magnitude enhancement of photoluminescence response with uniaxial tensile strain<sup>10</sup>. Another method to extrinsically tune optoelectronic properties has been achieved through application of external electric fields in WSe<sub>2</sub> and MoSe<sub>2</sub> monolayers<sup>11, 24</sup>. Yet, an intrinsic route to tune the electronic band structure and phonon dispersion relationship in these materials still remains unexplored.

Recently, the tunability of van der Waals interactions and anharmonic phonon scattering in bulk hexagonal boron nitride (*h*-BN) has been proven via experimental observation of changes in the electronic band gap and Raman signature due to the isotope effect<sup>25, 26</sup>. However, the isotopic effect on phonon and optoelectronic properties still remains unknown in the TMD class of atomically thin materials. Here, we report the isotopic engineering of optical band gap and phonon energy in atomically-thin CVD grown bilayer naturally abundant <sup>NA</sup>WNASe<sub>2</sub> and isotopically pure <sup>186</sup>W<sup>80</sup>Se<sub>2</sub> by combing X-ray diffraction and temperature-dependent Raman and photoluminescence spectroscopy from ~4 K to room temperature.

WSe<sub>2</sub> occurs naturally with five W isotopes<sup>27</sup> and six Se isotopes<sup>28</sup> with dominant concentrations of <sup>184</sup>W (30.64 %at.) and <sup>80</sup>Se (49.61 %at.). The strength of isotopic disorder in a compound is given by the 2<sup>nd</sup>-order mass variance parameter  $g = \sum_{i,j} [c_{i,j}(1-M_{i,j}/M_{i,avg})^2]$  in transport calculations<sup>29, 30</sup>, where  $c_{i,j}$  and  $M_{i,j}$  are the concentration and atomic mass of *i*-th atom and the *j*-th impurity, respectively, and  $M_{i,avg}$  is the average atomic mass. Naturally-occurring NAWNASe<sub>2</sub> has a molecular mass of 341.98u and g of 9.94×10<sup>-4</sup>, where u is the unified atomic mass constant. The g value can be reduced by more than 377 times to 2.63×10<sup>-6</sup> with a molecular mass of 345.99u through isotopic purification using <sup>186</sup>W and <sup>80</sup>Se at commercially available purification

levels greater than 99.9 %at., indicating that isotopic effects may play an important role in TMDs such as WSe<sub>2</sub> since the natural system is intrinsically disordered.

In this first work on the isotope effect in a TMD material, both naturally abundant NAWNASe<sub>2</sub> and isotopically pure <sup>186</sup>W<sup>80</sup>Se<sub>2</sub> bilayers were grown by chemical vapor deposition (CVD) on ~285 nm SiO<sub>2</sub>-coated silicon substrates similar to our previous report<sup>10</sup>. Since the optical band gap is extremely sensitive to strain and crystalline quality<sup>10, 31, 32</sup>, the NAWNASe<sub>2</sub> and <sup>186</sup>W<sup>80</sup>Se<sub>2</sub> bilayers are synthesized under identical growth conditions (for details see methods and supporting information), eliminating differences in structure caused by thermal expansion mismatch with the substrate<sup>33</sup>. To isolate the isotopic effect from the layer number<sup>19, 34</sup> and edge effect<sup>35</sup> contributions to the optical band gap, Figure 1a-c demonstrates our bilayer WSe<sub>2</sub> single crystals are synthesized so that the top and bottom layers have the same lateral dimensions. Atomic force microscopy (AFM) analysis shows a uniform thickness of ~1.3 nm over the entire crystallite for both NAWNASe<sub>2</sub> and 186W80Se<sub>2</sub> bilayers. Figure 1d-f illustrates that the Raman spectra of an isotopically pure bilayer <sup>186</sup>W<sup>80</sup>Se<sub>2</sub> crystallite is spatially uniform in intensity throughout the entire crystallite for the  $E_{2g}$ ,  $A_{1g}$  and  $A_{1g}^2$  Raman active modes, which is similar as our previous reported naturally abundant bilayer NAWNASe210. Photoluminescence (PL) also demonstrates spatially uniform peak intensity and in the entire crystallite (Figure 1g), further indicating the uniformity of atomic-level thickness. Room temperature X-ray diffraction (XRD) analysis for NAWNASe2 and <sup>186</sup>W<sup>80</sup>Se<sub>2</sub> are shown in Figure S1 of the supporting information. We have also conducted Rutherford backscattering spectrometry (RBS) analysis to obtain the elemental atomic ratios of the materials in this report. Analyzing the scattering yield ratios between W and Se, we obtain a W:Se ratio of 1:1.98 for both the naturally abundant and isotopically enriched samples indicating comparable stoichiometry and hence sample quality (Figure S2, supporting information).

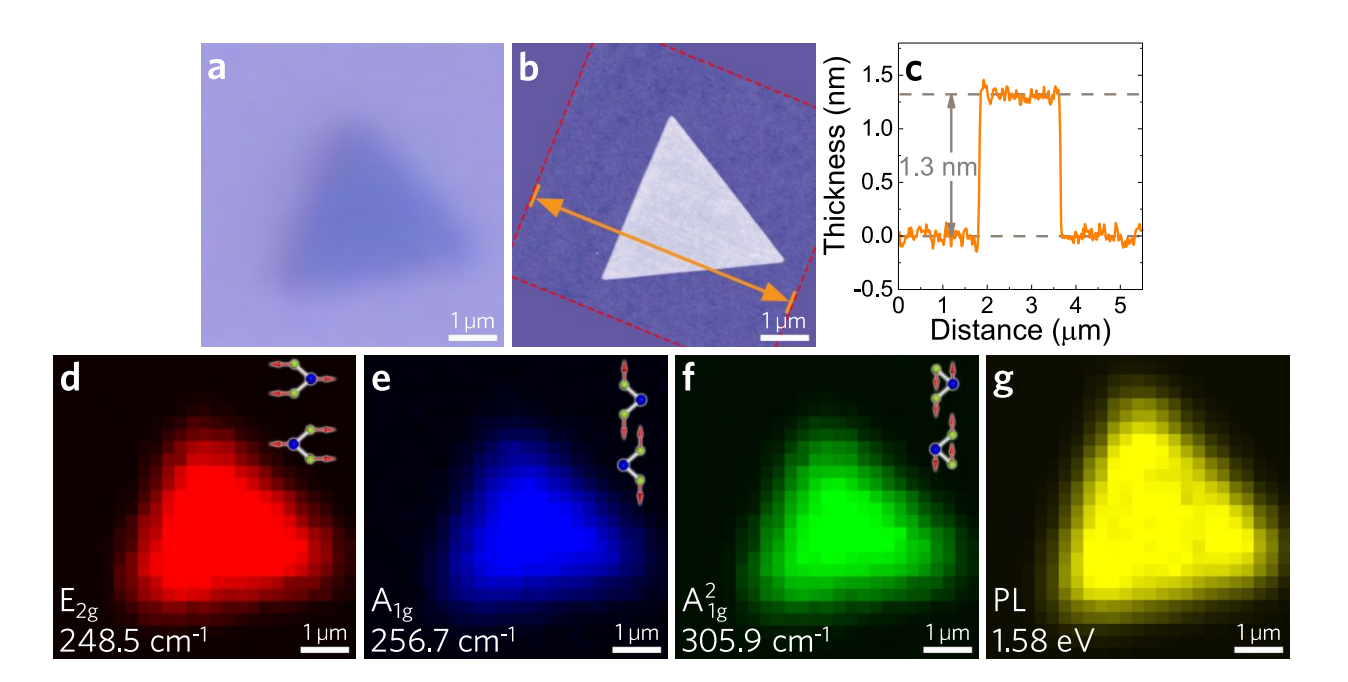


Figure 1. Spatially dependent characterization of an isotopically pure bilayer <sup>186</sup>W<sup>80</sup>Se<sub>2</sub> crystal.

(a) Optical image and (b) atomic force microscopy (AFM) characterization of <sup>186</sup>W<sup>80</sup>Se<sub>2</sub> on a 285 nm SiO<sub>2</sub>-on-Si substrate. (c) AFM height profile corresponding to line shown in (b). Spatially resolved Raman intensity at (d) 248.5 cm<sup>-1</sup> (E<sub>2g</sub> mode), (e) 256.7 cm<sup>-1</sup> (A<sub>1g</sub> mode), and (f) 305.9 cm<sup>-1</sup> (A<sup>2</sup><sub>1g</sub> mode), where the vibrational modes are depicted schematically. (g) Spatially resolved photoluminescence (PL) intensity at the peak emission wavelength of 1.58 eV.

Atomic vibrations described as phonons have energies which are dependent on the atomic mass, where frequency changes stemming from isotopic substitution can be monitored by Raman spectroscopy<sup>36</sup>. Figure 2a,b show the evolution of optical phonon energies with temperature in NAWNASe<sub>2</sub> and 186W80Se<sub>2</sub> bilayers using Raman spectroscopy and 532 nm laser excitation with a point-to-point resolution of ~0.51 cm<sup>-1</sup> using an 1800 gr/mm grating. To minimize the instrumental uncertainty, we conducted 6 sets of measurements with spectral windows defined by initial points differing by 0.1 cm<sup>-1</sup> to fully cover the point-to-point separation. The mean and standard deviation

of modeled peak positions and full width at half maximum (FWHM) obtained for each of these 6 spectra was used as the uncertainty for each data point. To avoid any influence from the slightly non-uniform temperature distribution on the sample mount in the optical cryostat, all Raman spectra were aligned using the silicon substrate peak at each nominal temperature.

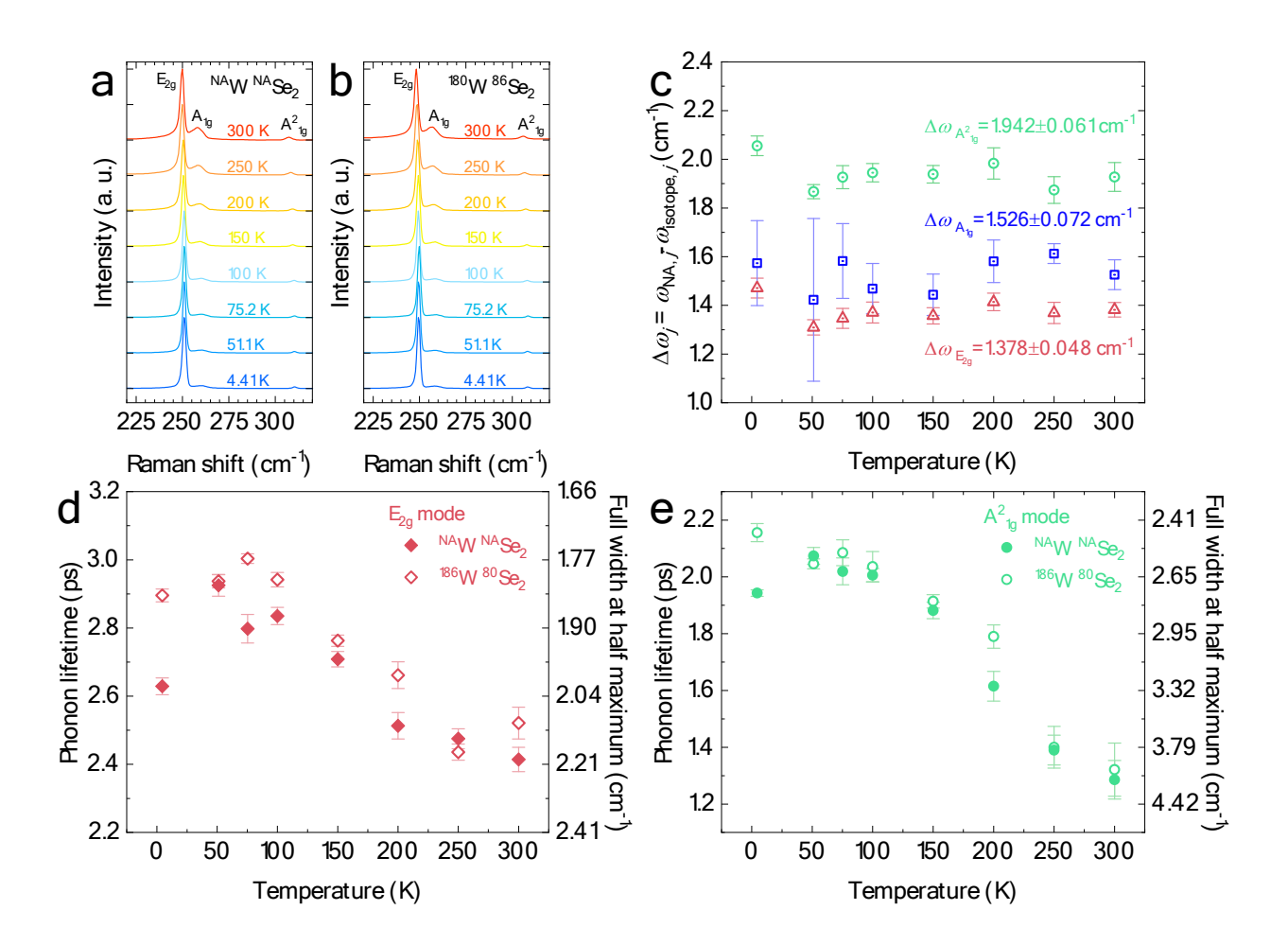


Figure 2. Isotopic mass dependent Raman spectra of bilayer WSe<sub>2</sub>. Normalized Raman spectra of (a) naturally abundant  $^{NA}W^{NA}Se_2$ , and (b) isotopically pure  $^{186}W^{80}Se_2$  over the temperature range from 4.41 to 300 K. (c) The phonon frequency difference (Δω) of  $E_{2g}$  (red),  $A_{1g}$  (blue) and  $A^2_{1g}$  (green) modes between  $^{NA}W^{NA}Se_2$  and  $^{186}W^{80}Se_2$ , where error is defined by the standard deviation of 6 measurements each with a different spectral window initial point in order to

minimize the instrument uncertainty. Temperature-dependent phonon lifetime and full width at half maximum of the (d)  $E_{2g}$  mode and (e)  $A^2_{1g}$  mode from 4.41 to 300 K.

The frequency of optical lattice vibrations is expected to decrease with heavier isotopic atomic mass according to a simple one-dimensional harmonic oscillator model<sup>37</sup> as  $\omega = [2C \cdot \Sigma_i M_i]$ <sup>1</sup>]<sup>1/2</sup> for zone center and  $\omega = (2C/M_i)^{1/2}$ , j = 1,2, for zone boundary phonons where C is the force constant and  $M_i$  is the mass of the j-th atom in the two-atom basis chain. The experimental frequency difference between NAWNASe2 and 186W80Se2 bilayers for each Raman active mode is evaluated as  $\Delta \omega_i = \omega_{i,NA} - \omega_{i,isotope}$ ,  $i = E_{2g}$ ,  $A_{1g}$ ,  $A_{1g}$ , where  $\omega_i$  is the Raman peak frequency of the i-th Raman active mode. Figure 2c shows that the phonon frequency globally red-shifts in the isotopic samples over the entire temperature range from 4.41 to 300 K. The E<sub>2g</sub> mode corresponds to intralayer tungsten and selenium atoms vibrating against each other in the hexagonal basal plane, in which the phonon frequency difference between  $^{NA}W^{NA}Se_2$  and  $^{186}W^{80}Se_2$  bilayers is  $\Delta \varpi_{E_{2g}}=$ 1.378±0.048 cm<sup>-1</sup>. The A<sub>1g</sub> mode represents selenium atom vibrations along the out-of-plane direction with  $\Delta\omega_{A_{1g}} = 1.526 \pm 0.072$  cm<sup>-1</sup>. The more interesting mode here is  $A_{1g}$  with  $\Delta\omega_{A_{1g}} =$  $1.942\pm0.061~\text{cm}^{-1}$ . The  $A_{1g}$  mode represents an interlayer vibration involving both tungsten and selenium atoms from different van der Waals layers, and only appears for two or more layers of WSe<sub>2</sub><sup>38</sup>. We observe that the isotopic effect on the interlayer out-of-plane A<sub>1g</sub> mode is larger than on the in-plane E<sub>2g</sub> mode or the intralayer out-of-plane A<sub>1g</sub> mode, which arises from the fact that the isotopic effect on the weak interlayer van der Waals interaction is larger than it is on the strong intralayer W-Se covalent interaction.

Besides the harmonic oscillation of phonons, the contribution of van der Waals bond length on phonon frequency also needs to be evaluated to support the statement above. The phonon frequency changes due to strain can be defined as  $^{10}$   $\Delta\omega_{i,\text{strain}} = -\varepsilon\gamma_i\omega_i$  where  $\gamma$  is the Grüneisen parameter,  $\varepsilon$  is the hydrostatic strain, and i represents the phonon mode. The interlayer van der Waals bond length change can be treated as  $\Delta c = \varepsilon_{zz}c$  where  $\Delta c$  is the c-lattice parameter change due to isotopic substitution, c is the natural abundance c-lattice parameter, and  $\varepsilon_{zz}$  is the out-of-plane strain component. Thus, the phonon frequency change due to isotopic substitution in this work can be approximated as  $\Delta\omega_{i,\text{strain}} = -\gamma_i\omega_i\Delta c/c$ . By adopting the experimental Grüneisen parameter of the  $A_{1g}$  mode in bilayer WSe<sub>2</sub> as  $0.357^{10}$  and the c-lattice parameters obtained from XRD analysis the phonon frequency changes expected due to isotope induced changes in van der Waals bond length can be estimated on the order of  $\Delta\omega_{A_{1g},\text{strain}} = 0.04$  cm<sup>-1</sup>, which is negligible compared to the measured experimental frequency changes.

The phonon lifetime is an important parameter that describes phonon scattering processes, and can be estimated from the FWHM of the Raman peak as<sup>26</sup>  $\tau = \hbar/\Gamma$  where  $\tau$  is the phonon lifetime,  $\hbar$  is the reduced Planck constant, and  $\Gamma$  is the FWHM. Figure 2d,e illustrates that isotopically pure <sup>186</sup>W<sup>80</sup>Se<sub>2</sub> exhibits slightly longer phonon lifetimes for both the intralayer inplane  $E_{2g}$  mode and the interlayer out-of-plane  $A_{1g}$  mode, although this is still only marginally higher than experimental uncertainty. The observed decrease of the phonon lifetime with temperature arises from an increase of phonon occupancy and phonon-phonon interaction with temperature<sup>39</sup>. At 4.41 (300) K, the phonon lifetime of the  $E_{2g}$  mode in bilayer <sup>186</sup>W<sup>80</sup>Se<sub>2</sub> is 2.90±0.02 (2.52±0.05) ps and ~2.16±0.03 (1.32±0.09) ps for the  $A_{1g}$  mode, which is 10.1 (4.42) % and 11.1 (2.77) % higher than the lifetimes of  $E_{2g}$  and  $A_{1g}$  modes in bilayer <sup>NA</sup>W<sup>NA</sup>Se<sub>2</sub>, respectively.

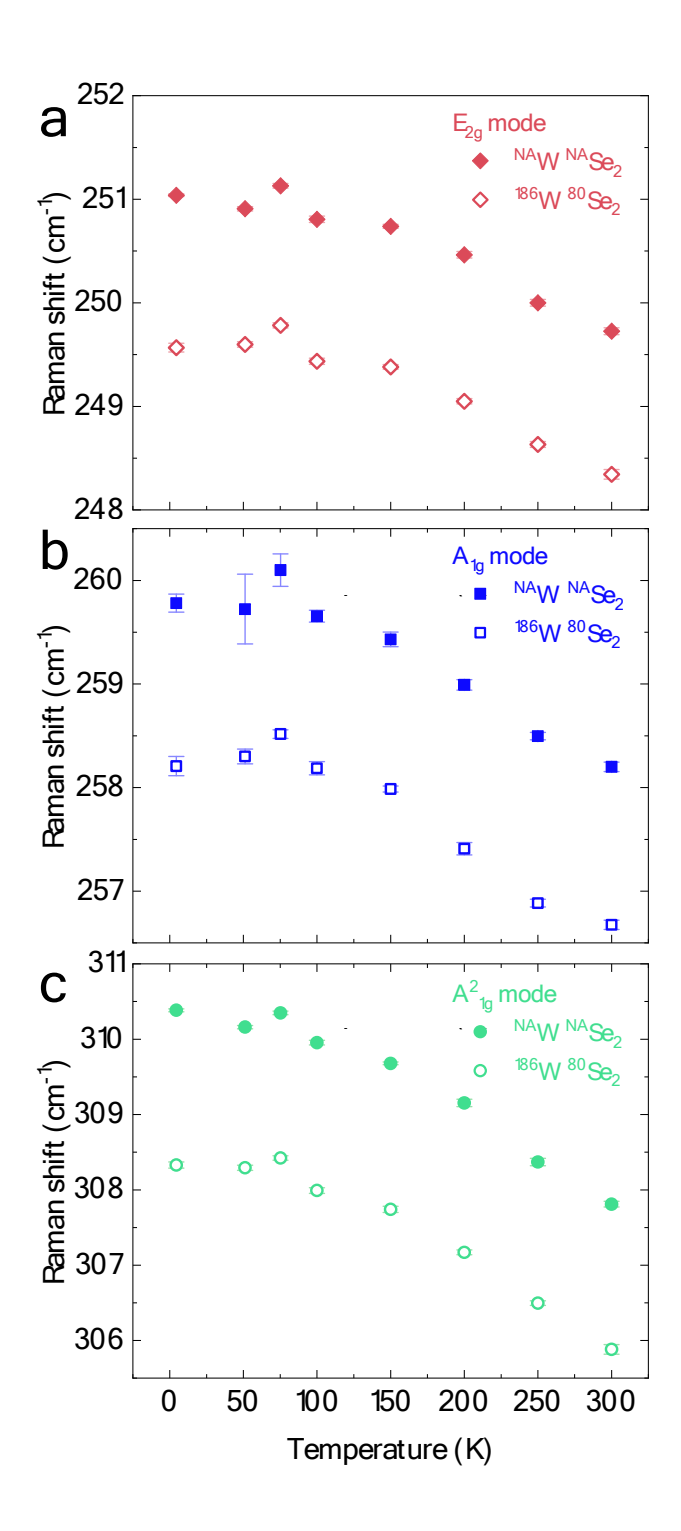
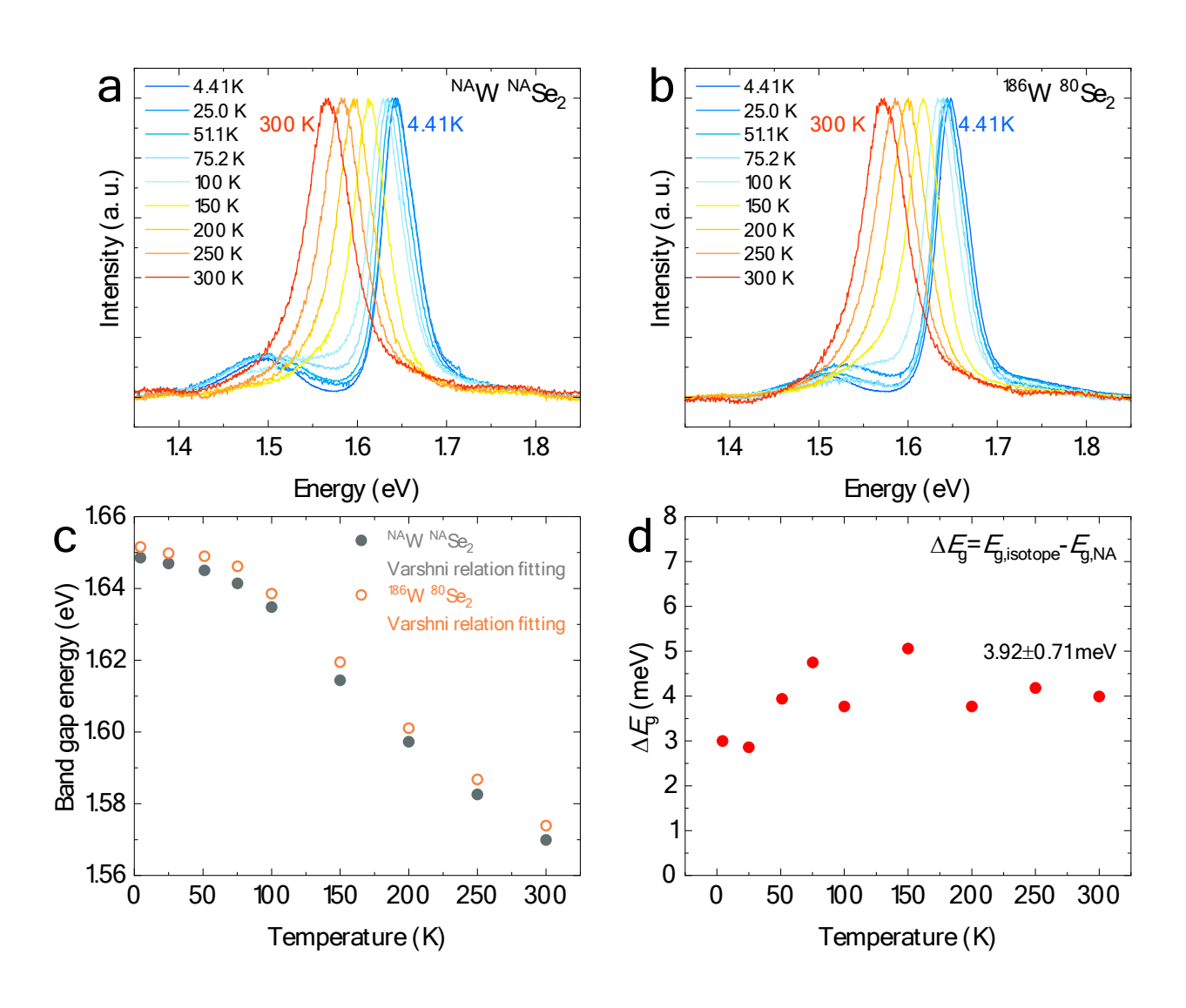


Figure 3. Temperature dependence of Raman active mode peak positions in isotopically engineered bilayer  $WSe_2$ . Raman shift for the (a)  $E_{2g}$ , (b)  $A_{1g}$ , and (c)  $A^2_{1g}$  modes of naturally abundant  $^{NA}W^{NA}Se_2$  (solid symbols) and isotopically pure  $^{186}W^{80}Se_2$  (open symbols).

Figure 3 shows the temperature dependent Raman shift of the  $E_{2g}$ ,  $A_{1g}$ , and  $A_{1g}$  modes of bilayer  $^{NA}W^{NA}Se_2$  and  $^{186}W^{80}Se_2$ . As the temperature increases from 4.41 to 300 K, the  $E_{2g}$  mode frequency decreases by  $1.313\pm0.025$  cm<sup>-1</sup> in  $^{NA}W^{NA}Se_2$  and by and  $1.223\pm0.031$  cm<sup>-1</sup> in  $^{186}W^{80}Se_2$ . The  $A_{1g}$  mode frequency drops a similar amount over the same temperature range,  $1.580\pm0.105$  cm<sup>-1</sup> and  $1.533\pm0.055$  cm<sup>-1</sup> in  $^{NA}W^{NA}Se_2$  and  $^{186}W^{80}Se_2$  respectively. The  $A_{1g}$  mode frequency drops by nearly twice as much,  $2.575\pm0.031$  cm<sup>-1</sup> and  $2.447\pm0.039$  cm<sup>-1</sup> in  $^{NA}W^{NA}Se_2$  and  $^{186}W^{80}Se_2$  bilayers respectively. This behavior can be explained by the positive thermal expansion coefficient (TEC) of both in-plane and out-of-plane unit cell parameters<sup>40, 41</sup>. We observe that the out-of-plane vibrational modes –  $A_{1g}$  and  $A_{1g}$  – have  $\sim$ 1.2 and  $\sim$ 1.9 times higher frequency changes than the in-plane vibration mode ( $E_{2g}$ ), respectively, which arises from an out-of-plane TEC approximately 1.6 times higher than the in-plane TEC<sup>41</sup>.

Electronic transitions from filled to empty states must conserve electron momentum. Bilayer  $WSe_2$  is known as a semiconductor with an indirect electronic band  $gap^{19}$ , in which the conduction band minimum at the  $\Sigma$ -point  $(CBM_{\Sigma})$  and valence band maximum at the K-point  $(VBM_K)$  are not at the same electron momentum in reciprocal space. Since the momentum of photons is negligible, especially in the wavelength range used in this work, the transition between  $CBM_{\Sigma}$  and  $VBM_K$  must involve phonon assistance to obey the rule of momentum conservation, which means the band gap can be affected by the isotope effect. Furthermore, phonon energy tuning by the isotope effect may also result from a change in wave vector arising from a shift of the PL band gap energy. Figure 4 reports the temperature dependent PL spectra for bilayer  $^{NA}W^{NA}Se_2$  and  $^{186}W^{80}Se_2$ . To avoid uncertainty arising from non-identical local heating by the excitation laser, all the samples were characterized under the same conditions including laser power and acquisition time at each temperature. Surprisingly, we observe a higher optical band

gap energy in bilayer  $^{186}\text{W}^{80}\text{Se}_2$  compared with bilayer  $^{NA}\text{W}^{NA}\text{Se}_2$  where the PL spectra of the isotopically pure sample blue-shifts by  $3.9 \pm 0.7$  meV over the entire temperature range from 4.41 to 300 K (Figure 4c). This trend is similar to the PL spectra blue-shift with increasing atomic mass phenomenon observed in other isotopically purified indirect band gap semiconductors, where the indirect band gap renormalization energy changes ~4.4 meV between  $h^{-10}\text{BN}$  and  $h^{-NA}\text{BN}^{25}$ , and ~2.2 meV between  $^{70}\text{Ge}$  and  $^{76}\text{Ge}^{42}$ .



*Figure 4. Isotopic mass dependent photoluminescence and optical band gap.* Normalized photoluminescence spectra over a temperature range from 4.41 to 300 K for (a) naturally abundant bilayer <sup>NA</sup>W<sup>NA</sup>Se<sub>2</sub>, and (b) isotopically pure bilayer <sup>186</sup>W<sup>80</sup>Se<sub>2</sub>. (c) Temperature dependence of the band gap of <sup>NA</sup>W<sup>NA</sup>Se<sub>2</sub> and <sup>186</sup>W<sup>80</sup>Se<sub>2</sub>, where modeling results using the empirical Varshni relation are given by solid and dashed lines, respectively. (d) Difference in optical band gap between <sup>NA</sup>W<sup>NA</sup>Se<sub>2</sub> and <sup>186</sup>W<sup>80</sup>Se<sub>2</sub> as a function of temperature.

The mechanisms responsible for this observable change in emission energy are indirect band gap renormalization<sup>43</sup> and isotopic phonon energy shift<sup>25</sup>. When evaluating the normalized electronic states in an indirect band gap semiconductor, the band gap renormalization energy is inversely proportional to the square root of effective mass and depends on the zero-point vibrational energy, calculated with all phonon modes at zero temperature. The isotope effect on indirect band gap renormalization energy has been proven in bulk h-BN<sup>25</sup>. However, the phonon replicas of MX<sub>2</sub> TMDs can only be obtained by resonant Raman spectroscopy, rather than the nonresonant spectra which is used here and in the previous h-BN report<sup>25</sup>. Another approach to estimate the renormalization energy is to extrapolate the linear relationship between temperature and band gap energy at high temperature, which is up to 800 K for bulk h-BN<sup>25</sup> and 1000 K for  $Ge^{43}$ . Comparing to h-BN, the atomically thin MX<sub>2</sub> TMDs are extremely sensitive to oxygen<sup>44</sup>, so there has been no available report of the PL spectra above 400 K of atomically thin WSe<sub>2</sub>. The band gap renormalization energy is proportional to  $\mu^{1/2}$ , and thus can be calculated as  $\delta E^{\alpha}$  =  $\delta E^{NA}(\mu^{\alpha}/\mu^{NA})^{1/2}$ , where  $\alpha$  represents the isotope and  $\mu$  indicates the reduced mass. Since both bilayer WSe<sub>2</sub> and WS<sub>2</sub> are indirect semiconductors, sharing the same lamellar structure and having similar band gaps, we adopt the experimental band gap renormalization energy of bilayer WS<sub>2</sub>

bilayer for bilayer  $^{NA}W^{NA}Se_2$ ,  $\delta E^{NA} \sim 500$  meV $^{45}$ . The change of band gap renormalization energy in the isotopically enriched sample can then be estimated as  $\delta E^{\alpha} - \delta E^{NA} \approx 2.992$  meV. Therefore, the isotopic band gap renormalization dominates the PL band gap shift which is measured as 3.9  $\pm$  0.7 meV in this study.

It is also important to evaluate the contribution of van der Waals bond length change to optical band gap energy, as out-of-plane compressive strain has been shown to decrease the indirect optical band gap energy in bilayer WSe<sub>2</sub><sup>10</sup>. A similar trend has also been predicted for bilayer MoS<sub>2</sub>, in which the indirect band gap decreases with shorter c-lattice parameter<sup>46</sup>. This is contrary to our observation of the higher optical band gap in bilayer <sup>186</sup>W<sup>80</sup>Se<sub>2</sub> which possesses a smaller c-lattice parameter than NAWNASe2. Therefore, we conclude that the van der Waals bond length is not the dominant factor resulting in the optical band gap energy change with isotopic purification in this work. The temperature evolution of the optical band gap is shown in Figure 4d, which decreases from 1.649 eV at 4.41 K to 1.599 eV at 300 K for NAWNASe2 and from 1.652 eV at 4.41 K to 1.574 eV at 300 K for <sup>186</sup>W<sup>80</sup>Se<sub>2</sub>. This behavior can be modeled using the empirical Varshni relation<sup>47</sup> as  $E_{\rho}(T) = E_{\rho}(T=0) - (\alpha T^2)/(\beta + T)$  where  $E_{\rho}(T=0)$  is the band gap energy at 0 K, T is the absolute temperature, and  $\alpha$  and  $\beta$  are adjustable constants. We obtained  $E_{\sigma}(T=0)=1.6504$ eV,  $\alpha = 0.365$  meV/K, and  $\beta = 93.926$  K for NAWNASe<sub>2</sub>, and  $E_g(T=0)=1.6539$  eV,  $\alpha = 0.379$  meV/K and  $\beta = 112.964$  K for  $^{186}W^{80}Se_2$ . Coefficients of determination were 0.991 and 0.992 for NAWNASe<sub>2</sub> and <sup>186</sup>W<sup>80</sup>Se<sub>2</sub>, respectively. The slight difference between our experimental data and the empirical modeling at low temperature arises from the quadratic temperature dependence of the empirical Varshni relation, whereas theoretical and experimental observations are reported to exhibit  $T^4$  dependence at low temperature<sup>43, 48, 49</sup>.

In conclusion, we have experimentally demonstrated the isotope effect on the phonon frequency, phonon lifetime, and optical band gap energy in an atomically thin TMD through temperature dependent spectroscopy of naturally abundant and isotopically pure bilayer WSe<sub>2</sub>. We have postulated a new mechanism by which the electronic band gap energy and phonon dispersion can be tuned in this material by isotopic enrichment. The outcomes of this study should help stimulate future investigations and theoretical predictions of phonon and electronic property modification in other isotopically enriched van der Waals material systems, such as the isotope effect on thermal conductivity<sup>36, 50-53</sup>.

#### Supporting information available

Additional synthesis, structural characterization, and experimental details. This material is available free of charge via the Internet at http://pubs.acs.org.

# Acknowledgment

This project was conceived and led by M.T.P.; W.W. and M.T.P. conducted WSe<sub>2</sub> synthesis, experimental characterizations, and analytical modeling; W.W. and M.D.D. performed X-ray diffraction spectroscopy and analysis. The manuscript was written by M.T.P. and W.W. with contributions from all authors. This work was supported by the U.S. National Science Foundation under Award No. CAREER-1553987 (M.T.P., W.W.). This work was performed, in part, at the Center for Integrated Nanotechnologies, an Office of Science User Facility operated for the U.S. Department of Energy (DOE) Office of Science. Los Alamos National Laboratory, an affirmative action equal opportunity employer, is managed by Triad National Security, LLC for

the U.S. Department of Energy's NNSA, under contract 89233218CNA000001. This work was performed, in part, at the Harvard University Center for Nanoscale Systems (CNS), a member of the National Nanotechnology Coordinated Infrastructure Network (NNCI), which is supported by the U.S. National Science Foundation under Award No. 1541959.

#### References

- (1) Novoselov, K. S.; Geim, A. K.; Morozov, S. V.; Jiang, D.; Zhang, Y.; Dubonos, S. V.; Grigorieva, I. V.; Firsov, A. A. Electric field effect in atomically thin carbon films, *Science* **2004**, *306*, 666–669.
- (2) Geim, A. K.; Grigorieva, I. V. Van der Waals heterostructures, *Nature* **2013**, *499*, 419-425.
- (3) Chhowalla, M.; Shin, H. S.; Eda, G.; Li, L.-J.; Loh, K. P.; Zhang, H. The chemistry of two-dimensional layered transition metal dichalcogenide nanosheets, *Nat. Chem.* **2013**, *5*, 263-275.
- (4) Bhimanapati, G. R.; Lin, Z.; Meunier, V.; Jung, Y.; Cha, J.; Das, S.; Xiao, D.; Son, Y.; Strano, M. S.; Cooper, V. R.; Liang, L.; Louie, S. G.; Ringe, E.; Zhou, W.; Kim, S. S.; Naik, R. R.; Sumpter, B. G.; Terrones, H.; Xia, F.; Wang, Y.; Zhu, J.; Akinwande, D.; Alem, N.; Schuller, J. A.; Schaak, R. E.; Terrones, M.; Robinson, J. A. Recent advances in two-dimensional materials beyond graphene, *ACS Nano* **2015**, *9*, 11509–11539.
- (5) Zhou, H.; Wang, C.; Shaw, J. C.; Cheng, R.; Chen, Y.; Huang, X.; Liu, Y.; Weiss, N. O.; Lin, Z.; Huang, Y.; Duan, X. Large area growth and electrical properties of p-type WSe<sub>2</sub> atomic layers, *Nano Lett.* **2015**, *15*, 709–713.
- (6) Mak, K. F.; Shan, J. Photonics and optoelectronics of 2D semiconductor transition metal dichalcogenides, *Nat. Photonics* **2016**, *10*, 216–226.
- (7) Schaibley, J. R.; Yu, H.; Clark, G.; Rivera, P.; Ross, J. S.; Seyler, K. L.; Yao, W.; Xu, X. Valleytronics in 2D materials, *Nat. Rev. Mater.* **2016**, *1*, 16055-1–15.
- (8) Lee, C.-H.; Lee, G.-H.; van der Zande, A. M.; Chen, W.; Li, Y.; Han, M.; Cui, X.; Arefe, G.; Nuckolls, C.; Heinz, T. F.; Guo, J.; Hone, J.; Kim, P. Atomically thin p–n junctions with van der Waals heterointerfaces, *Nat. Nanotechnol.* **2014**, *9*, 676–681.
- (9) Huang, C.; Wu, S.; Sanchez, A. M.; Peters, J. J. P.; Beanland, R.; Ross, J. S.; Rivera, P.; Yao, W.; Cobden, D. H.; Xu, X. Lateral heterojunctions within monolayer MoSe<sub>2</sub>–WSe<sub>2</sub> semiconductors, *Nat. Mater.* **2014**, *13*, 1096–1101.

- (10) Wu, W.; Wang, J.; Ercius, P.; Wright, N. C.; Leppert-Simenauer, D. M.; Burke, R. A.; Dubey, M.; Dongare, A. M.; Pettes, M. T. Giant mechano-optoelectronic effect in an atomically thin semiconductor, *Nano Lett.* **2018**, *18*, 2351–2357.
- (11) Chakraborty, C.; Kinnischtzke, L.; Goodfellow, K. M.; Beams, R.; Vamivakas, A. N. Voltage-controlled quantum light from an atomically thin semiconductor, *Nat. Nanotechnol.* **2015**, *10*, 507–511.
- (12) Tonndorf, P.; Schmidt, R.; Schneider, R.; Kern, J.; Buscema, M.; Steele, G. A.; Castellanos-Gomez, A.; van der Zant, H. S. J.; Michaelis de Vasconcellos, S.; Bratschitsch, R. Single-photon emission from localized excitons in an atomically thin semiconductor, *Optica* **2015**, *2*, 347–352.
- (13) Palacios-Berraquero, C.; Barbone, M.; Kara, D. M.; Chen, X.; Goykhman, I.; Yoon, D.; Ott, A. K.; Beitner, J.; Watanabe, K.; Taniguchi, T.; Ferrari, A. C.; Atatüre, M. Atomically thin quantum light-emitting diodes, *Nat. Commun.* **2016**, *7*, 12978-1–6.
- (14) Branny, A.; Kumar, S.; Proux, R.; Gerardot, B. D. Deterministic strain-induced arrays of quantum emitters in a two-dimensional semiconductor, *Nat. Commun.* **2017**, *8*, 15053-1–7.
- (15) Palacios-Berraquero, C.; Kara, D. M.; Montblanch, A. R. P.; Barbone, M.; Latawiec, P.; Yoon, D.; Ott, A. K.; Loncar, M.; Ferrari, A. C.; Atatüre, M. Large-scale quantum-emitter arrays in atomically thin semiconductors, *Nat. Commun.* **2017**, *8*, 15093-1–6.
- (16) He, Y.-M.; Clark, G.; Schaibley, J., R.; He, Y.; Chen, M.-C.; Wei, Y.-J.; Ding, X.; Zhang, Q.; Yao, W.; Xu, X.; Lu, C.-Y.; Pan, J.-W. Single quantum emitters in monolayer semiconductors, *Nat. Nanotechnol.* **2015**, *10*, 497–502.
- (17) Iannaccone, G.; Bonaccorso, F.; Colombo, L.; Fiori, G. Quantum engineering of transistors based on 2D materials heterostructures, *Nat. Nanotechnol.* **2018**, *13*, 183–191.
- (18) Mak, K. F.; Lee, C.; Hone, J.; Shan, J.; Heinz, T. F. Atomically thin MoS<sub>2</sub>: A new direct-gap semiconductor, *Phys. Rev. Lett.* **2010**, *105*, 136805-1-4.
- (19) Zhao, W.; Ghorannevis, Z.; Chu, L.; Toh, M.; Kloc, C.; Tan, P.-H.; Eda, G. Evolution of electronic structure in atomically thin sheets of WS<sub>2</sub> and WSe<sub>2</sub>, ACS Nano **2013**, 7, 791-797.
- (20) Yazdani, S.; Pettes, M. T. Nanoscale self-assembly of thermoelectric materials: A review of chemistry-based approaches, *Nanotechnology* **2018**, *29*, 432001-1–43.
- (21) Conley, H. J.; Wang, B.; Ziegler, J. I.; Haglund, R. F.; Pantelides, S. T.; Bolotin, K. I. Bandgap engineering of strained monolayer and bilayer MoS<sub>2</sub>, *Nano Lett.* **2013**, *13*, 3626-3630.

- (22) Desai, S. B.; Seol, G.; Kang, J. S.; Fang, H.; Battaglia, C.; Kapadia, R.; Ager, J. W.; Guo, J.; Javey, A. Strain-induced indirect to direct bandgap transition in multilayer WSe<sub>2</sub>, *Nano Lett.* **2014**, *14*, 4592–4597.
- (23) Dai, Z.; Liu, L.; Zhang, Z. Strain engineering of 2D materials: Issues and opportunities at the interface, *Adv. Mater.* **2019**, *Early View*, DOI: 10.1002/adma.201805417.
- (24) He, K.; Poole, C.; Mak, K. F.; Shan, J. Experimental demonstration of continuous electronic structure tuning via strain in atomically thin MoS<sub>2</sub>, *Nano Lett.* **2013**, *13*, 2931-2936.
- (25) Vuong, T. Q. P.; Liu, S.; Van der Lee, A.; Cuscó, R.; Artús, L.; Michel, T.; Valvin, P.; Edgar, J. H.; Cassabois, G.; Gil, B. Isotope engineering of van der Waals interactions in hexagonal boron nitride, *Nat. Mater.* **2017**, *17*, 152–158.
- (26) Cuscó, R.; Artús, L.; Edgar, J. H.; Liu, S.; Cassabois, G.; Gil, B. Isotopic effects on phonon anharmonicity in layered van der Waals crystals: Isotopically pure hexagonal boron nitride, *Phys. Rev. B* **2018**, *97*, 155435-1–12.
- (27) Völkening, J.; Köppe, M.; Heumann, K. G. Tungsten isotope ratio determinations by negative thermal ionization mass spectrometry, *Int. J. Mass Spectrom. Ion Proc.* **1991**, *107*, 361-368.
- (28) Wachsmann, M.; Heumann, K. G. Negative thermal ionization mass spectroscopy of main group elements Part 2. 6th group: Sulfur, selenium and tellurium, *Int. J. Mass Spectrom.* **1992**, *114*, 209–220.
- (29) Klemens, P. G. The scattering of low-frequency lattice waves by static imperfections, *Proc. Phys. Soc. A* **1955**, *68*, 1113–1128.
- (30) Tamura, S. Isotope scattering of dispersive phonons in Ge, Phys. Rev. B 1983, 27, 858-866.
- (31) Schmidt, R.; Niehues, I.; Schneider, R.; Drüppel, M.; Deilmann, T.; Rohlfing, M.; Michaelis de Vasconcellos, S.; Castellanos-Gomez, A.; Bratschitsch, R. Reversible uniaxial strain tuning in atomically thin WSe<sub>2</sub>, *2D Mater.* **2016**, *3*, 021011-1–7.
- (32) Liu, Z.; Amani, M.; Najmaei, S.; Xu, Q.; Zou, X.; Zhou, W.; Yu, T.; Qiu, C.; Birdwell, A. G.; Crowne, F. J.; Vajtai, R.; Yakobson, B. I.; Xia, Z.; Dubey, M.; Ajayan, P. M.; Lou, J. Strain and structure heterogeneity in MoS<sub>2</sub> atomic layers grown by chemical vapour deposition, *Nat. Commun.* **2014**, *5*, 5246.
- (33) Ahn, G. H.; Amani, M.; Rasool, H.; Lien, D.-H.; Mastandrea, J. P.; Ager Iii, J. W.; Dubey, M.; Chrzan, D. C.; Minor, A. M.; Javey, A. Strain-engineered growth of two-dimensional materials, *Nat. Commun.* **2017**, *8*, 608-1–8.

- (34) Tonndorf, P.; Schmidt, R.; Böttger, P.; Zhang, X.; Börner, J.; Liebig, A.; Albrecht, M.; Kloc, C.; Gordan, O.; Zahn, D. R. T.; Michaelis de Vasconcellos, S.; Bratschitsch, R. Photoluminescence emission and Raman response of monolayer MoS<sub>2</sub>, MoSe<sub>2</sub>, and WSe<sub>2</sub>, *Opt. Express* **2013**, *21*, 4908–4916.
- (35) Dong, L.; Wang, J.; Namburu, R.; O'Regan, T. P.; Dubey, M.; Dongare, A. M. Edge effects on band gap energy in bilayer 2H-MoS<sub>2</sub> under uniaxial strain, *J. Appl. Phys.* **2015**, *117*, 244303.
- (36) Pettes, M. T.; Ji, H. X.; Sadeghi, M. M.; Jo, I.; Wu, W.; Ruoff, R. S.; Shi, L. Scattering of phonons by high-concentration isotopic impurities in ultrathin graphite, *Phys. Rev. B* **2015**, *91*, 035429-1–13.
- (37) Kittel, C. Introduction to Solid State Physics. 8th ed.; John Wiley & Sons: New York, 2005.
- (38) Terrones, H.; Corro, E. D.; Feng, S.; Poumirol, J. M.; Rhodes, D.; Smirnov, D.; Pradhan, N. R.; Lin, Z.; Nguyen, M. A. T.; Elías, A. L.; Mallouk, T. E.; Balicas, L.; Pimenta, M. A.; Terrones, M. New first order Raman-active modes in few layered transition metal dichalcogenides, *Sci. Rep.* **2014**, *4*, 4215-1–9.
- (39) Beechem, T.; Graham, S. Temperature and doping dependence of phonon lifetimes and decay pathways in GaN, *J. Appl. Phys.* **2008**, *103*, 093507-1–8.
- (40) Hu, X.; Yasaei, P.; Jokisaari, J.; Öğüt, S.; Salehi-Khojin, A.; Klie, R. F. Mapping thermal expansion coefficients in freestanding 2D materials at the nanometer scale, *Phys. Rev. Lett.* **2018**, *120*, 055902-1–6.
- (41) Murray, R.; Evans, B. The thermal expansion of  $2H-MoS_2$  and  $2H-WSe_2$  between 10 and 320 K, *J. Appl. Cryst.* **1979**, *12*, 312–315.
- (42) Etchegoin, P.; Weber, J.; Cardona, M.; Hansen, W. L.; Itoh, K.; Haller, E. E. Isotope effect in Ge: A photoluminescence study, *Solid State Commun.* **1992**, *83*, 843–848.
- (43) Cardona, M.; Thewalt, M. L. W. Isotope effects on the optical spectra of semiconductors, *Rev. Mod. Phys.* **2005**, *77*, 1173–1224.
- (44) Kang, K.; Godin, K.; Kim, Y. D.; Fu, S.; Cha, W.; Hone, J.; Yang, E.-H. Graphene-assisted antioxidation of tungsten disulfide monolayers: Substrate and electric-field effect, *Adv. Mater.* **2017**, *29*, 1603898-1–8.
- (45) Chernikov, A.; Ruppert, C.; Hill, H. M.; Rigosi, A. F.; Heinz, T. F. Population inversion and giant bandgap renormalization in atomically thin WS<sub>2</sub> layers, *Nat. Photonics* **2015**, *9*, 466–470.

- (46) Cao, B.; Li, T. Interlayer electronic coupling in arbitrarily stacked MoS<sub>2</sub> bilayers controlled by interlayer S–S interaction, *J. Phys. Chem. C* **2015**, *119*, 1247–1252.
- (47) Varshni, Y. P. Temperature dependence of the energy gap in semiconductors, *Physica* **1967**, *34*, 149–154.
- (48) Cardona, M.; Kremer, R. K. Temperature dependence of the electronic gaps of semiconductors, *Thin Solid Films* **2014**, *571*, 680–683.
- (49) Lautenschlager, P.; Allen, P. B.; Cardona, M. Temperature dependence of band gaps in Si and Ge, *Phys. Rev. B* **1985**, *31*, 2163–2171.
- (50) Wu, X.; Yang, N.; Luo, T. Unusual isotope effect on thermal transport of single layer molybdenum disulphide, *Appl. Phys. Lett.* **2015**, *107*, 191907-1–5.
- (51) Chen, S.; Wu, Q.; Mishra, C.; Kang, J.; Zhang, H.; Cho, K.; Cai, W.; Balandin, A. A.; Ruoff, R. S. Thermal conductivity of isotopically modified graphene, *Nat. Mater.* **2012**, *11*, 203-207.
- (52) Lindsay, L.; Broido, D. A. Enhanced thermal conductivity and isotope effect in single-layer hexagonal boron nitride, *Phys. Rev. B* **2011**, *84*, 155421-1–6.
- (53) Li, X.; Zhang, J.; Puretzky, A. A.; Yoshimura, A.; Sang, X.; Cui, Q.; Li, Y.; Liang, L.; Ghosh, A. W.; Zhao, H.; Unocic, R. R.; Meunier, V.; Rouleau, C. M.; Sumpter, B. G.; Geohegan, D. B.; Xiao, K. Isotope-Engineering the Thermal Conductivity of Two-Dimensional MoS<sub>2</sub>, *ACS Nano* **2019**, *Article ASAP*, DOI: 10.1021/acsnano.8b09448.

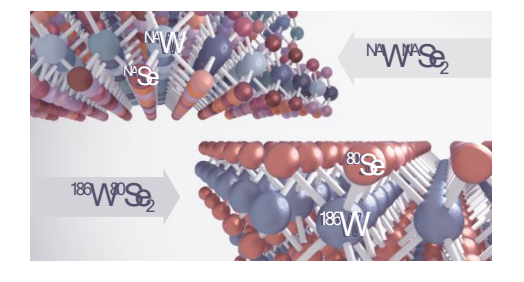


Table of Contents Graphic.

